

SEARCH FOR SOMETHING

by

Joaquin Emilio Siado Castañeda

A DISSERTATION

Presented to the Faculty of

The Graduate College at the University of Nebraska

In Partial Fulfilment of Requirements

For the Degree of Doctor of Philosophy

Major: Physics and Astronomy

Under the Supervision of Professor Daniel Claes

Lincoln, Nebraska

July, 2020

SEARCH FOR SOMETHING

Joaquin Emilio Siado Castañeda, Ph.D.

University of Nebraska, 2020

Advisers: Dan Claes and Aaron Dominguez

my abstract

ACKNOWLEDGMENTS

Many people has contributed to make this work possible that it is impossible to name them all.

Table of Contents

| | |
|--|------|
| List of Figures | viii |
| List of Tables | x |
| 1 Introduction | 1 |
| 2 The LHC Accelerator and the CMS Experiment | 2 |
| 2.1 The LHC Accelerator | 2 |
| 2.2 CMS | 4 |
| 2.2.1 The Tracker Detector | 4 |
| 2.2.1.1 Pixel Detector | 4 |
| 2.2.1.2 Silicon Strips | 4 |
| 2.2.2 The Electromagnetic Calorimeter | 4 |
| 2.2.3 The Hadronic Calorimeter | 4 |
| 2.2.4 The Muon Chambers | 4 |
| 3 The SM and BSM Theories | 9 |
| 4 Event generation, simulation and reconstruction | 10 |
| 5 Search for the particle | 11 |

| | |
|--|-----------|
| 6 More on the Analysis? | 12 |
| 7 Module Production for the Phase I CMS Pixel Detector Upgrade | 13 |
| 7.1 The CMS Pixel Detector Phase I Upgrade | 14 |
| 7.2 Module Production at UNL | 14 |
| 7.2.1 Visual Inspections | 16 |
| 7.2.2 IV Test | 19 |
| 7.2.3 Gluing | 20 |
| 7.2.4 Wirebonding | 21 |
| 7.2.5 Encapsulation | 21 |
| 7.2.6 Electrical Test of a Fully assembly Module | 23 |
| 7.2.6.1 IV Test | 26 |
| 7.2.6.2 Pretest | 26 |
| 7.2.6.3 Pixel Alive | 27 |
| 7.2.6.4 Trimming Test | 29 |
| 7.2.6.5 PH Optimization | 30 |
| 7.2.6.6 Gain Pedestal | 30 |
| 7.2.6.7 Scurve Test | 30 |
| 7.2.6.8 Bond Bonding Test | 31 |
| 7.2.6.9 Summary | 32 |
| 8 Beam Test of the RD53 chip for CMS Pixel Detector Upgrade Phase 2 | 35 |
| 8.1 Introduction | 35 |
| 8.2 The RD53 Chip | 35 |
| 8.3 Purpose of Test Beam | 35 |
| 8.4 Test Beam Set Up | 35 |

| | | |
|----------|---------------------|-----------|
| 8.5 | Results | 35 |
| 9 | Conclusions | 36 |
| 9.1 | Analysis | 36 |
| 9.2 | Phase 1 | 36 |
| 9.3 | Beam Test | 36 |
| | References | 37 |

List of Figures

| | | |
|------|---|----|
| 2.1 | The CERN acceleration <i>facilities</i> | 3 |
| 2.2 | LHC luminosity | 4 |
| 2.3 | LHC dipoles | 5 |
| 2.4 | CMS cross sectional view | 6 |
| 2.5 | CMS Tracking system. | 7 |
| 2.6 | CMS cross sectional view | 7 |
| 2.7 | CMS cross sectional view | 8 |
| 7.1 | Expected performance of the original pixel detector for different luminosities. | 15 |
| 7.2 | Layout of the upgraded and old pixel detectors. | 15 |
| 7.3 | UNL module assembly workflow | 16 |
| 7.4 | Photograph of a BBM and HDI. | 17 |
| 7.5 | Photograph of the visual inspection and IV test station. | 18 |
| 7.6 | Visual inspection of a bare module. | 18 |
| 7.7 | Visual inspection of a HDI. | 19 |
| 7.8 | IV test of BBM | 20 |
| 7.9 | Gluing and encapsulation set up | 21 |
| 7.10 | Gluing result | 22 |

| | | |
|------|---|----|
| 7.11 | wirebonder machine | 22 |
| 7.12 | Wirebonded module | 23 |
| 7.13 | Encapsulation materials | 23 |
| 7.14 | Encapsulation results | 24 |
| 7.15 | Fully assembly Module | 25 |
| 7.16 | Testing set up | 25 |
| 7.17 | IV results of a module | 26 |
| 7.18 | Programable ROC and working point | 27 |
| 7.19 | Pixel alive test | 28 |
| 7.20 | Faulty pixel alive test | 28 |
| 7.21 | Trim test turn on | 30 |
| 7.22 | Trim test Trim bits | 31 |
| 7.23 | Trim test final | 32 |
| 7.24 | Scurve test | 33 |
| 7.25 | Bond bonding test. | 33 |
| 7.26 | Pixel unit cell. | 34 |

List of Tables

CHAPTER 1

Introduction

Talk about particle physics in general and the organization of the documents

CHAPTER 2

The LHC Accelerator and the CMS Experiment

In the 1960s Peter Higgs and others *need ref* put up the finishing touches on a theory combining three of the four fundamental forces. This theory became to be known as the Standard Model (SM) of particles physics. It predicted the existence of several particles which were discovered in the following decades. However, one particle was proving to be elusive, the so-called Higgs boson. With this in mind the European Organization for Nuclear Research (CERN) started plans to build an accelerator large enough to be able to find this elusive particle. Hence, the Large Hadron Collider (LHC) was born.

2.1 The LHC Accelerator

A circular ring of 27 Km in circumference, the LHC was built at the French-Swiss border outside Geneva, Switzerland, see figure 2.1.

Four experiments were designed and build to test different physics theories and search for undiscovered particles at the LHC. Two of them, A Toroidal Large Aparatus (ATLAS) [1] and the Compact Muon Solenoid (CMS) [2] are large multipurpose experiments. The third experiment is LHCb [3], which is specifically dedicated to study B-meson physics, the last experiment ALICE [4], A Large Ion Collider Experiment,

**CUANDO QUEDAS CON UN AMIGO EN IR
A HACER EJERCICIO A LAS 6:00am.
PERO AMBOS DUERMEN TRANQUILOS
PORQUE SABEN:
QUE ESO NUNCA SUCEDERÁ.**



Figure 2.1: The CERN acceleration *facilities* showing the location of the four main experiment as well as the acceleration process[need ref].

was design to investigate heavy ion collisions.

Four experiments were designed and build to test different physics theories and search for undiscovered particles at the LHC. Two of them, A Toroidal Large Aparatus (ATLAS) [1] and the Compact Muon Solenoid (CMS) [2] are large multipurpose experiments. The third experiment is LHCb [3], which is specifically dedicated to study B-meson physics, the last experiment ALICE [4], A Large Ion Collider Experiment, was design to investigate heavy ion collisions.

Cuando eres el único que no se ha descargado #TikTok en esta #cuarentena



Figure 2.2: LHC luminosity.

2.2 CMS

2.2.1 The Tracker Detector

2.2.1.1 Pixel Detector

2.2.1.2 Silicon Strips

2.2.2 The Electromagnetic Calorimeter

2.2.3 The Hadronic Calorimeter

2.2.4 The Muon Chambers



Figure 2.3: LHC dipoles.

Las 3 etapas de la tesis.

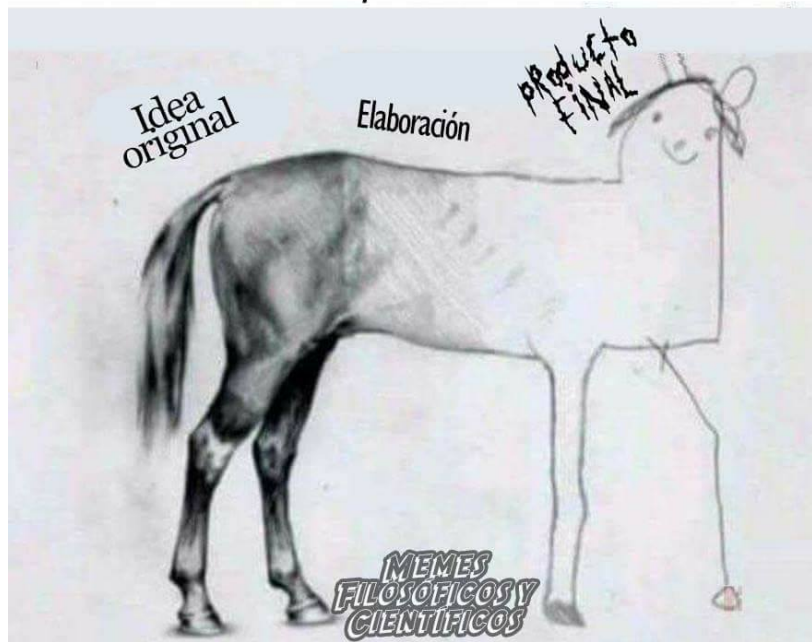


Figure 2.4: CMS cross sectional view.



Figure 2.5: CMS Tracking system.



Figure 2.6: CMS cross sectional view.



Figure 2.7: CMS cross sectional view.

CHAPTER 3

The SM and BSM Theories

Proposed in the 1960s the standard model of particles physics has been successful in describing many phenomena of the particle world

CHAPTER 4

Event generation, simulation and reconstruction

Description of event generation and simulation

CHAPTER 5

Search for the particle

Data analysis details

CHAPTER 6

More on the Analysis?

More?

CHAPTER 7

Module Production for the Phase I CMS Pixel Detector Upgrade

As discussed in chapter 2 the CMS pixel detector will *suffer* from radiation damage throughout its lifetime hence the need for periodical updates. The first version of the detector was known as phase 0, it became fully operational 2010 after solving a setback during the original starting period in 2008. In 2017 the pixel detector was replaced during the so-called phase 1 upgrade, the University of Nebraska, high energy group (UNL-HEP) played a major role in assembling and testing over 500 modules, from 2013 to 2016, which then became part of the forward region of the pixel detector (FPix). The next update of this detector (phase 2) is projected to take place in 2025 when the current detector will be reaching its limits. In this chapter we describe why the phase 0 pixel detector needed an upgrade making the work done by the UNL-HEP group. Some of these steps will be highlighted and described in detail as they were my contributions to this production campaign. Specially the and highlighting

7.1 The CMS Pixel Detector Phase I Upgrade

The CMS pixel detector is composed of two sections, the barrel section (BPix) and the forward section (FPix). Each of these sections (for phase 0) was composed of three layers originally designed to record three 3D positions (tracks) of the particles emerging from the pp collisions. As well as to provide information to reconstruct primary and secondary vertices of decaying particles. This detector performed well during the LHC run I,^{incorporate the bunch crossing?} taking data at the design luminosity of $1 \times 10^{34} cm^{-2}s^{-1}$, which was then used in many analysis including the discovery of the Higgs boson published in 2013. But after a few years of operation the pixel detector started to degrade due to radiation damage, causing an increase of fake rates as well as loose on resolution. Moreover, for run II the LHC planned to double the luminosity with successive increment until reach its peak of $2 \times 10^{35} cm^{-2}s^{-1}$. A simulation of the performance of the pixel detector under different luminosity conditions can be seen in figure 7.1

This degradation prompted the need for an improved pixel detector. It was designed to have four layers in the barrel ubicated at distances of $H_{\text{en}}=2420$ and 3 layers at each endcap as shown in 7.2. better

7.2 Module Production at UNL

The UNL module production workflow was designed to follow a pipeline-like structure as shown in figure 7.3. This allows for different batches of modules to be going through it at different stages without stopping the workflow. Following is a short description of the tests and procedures performed during the production in the UNL silicon Lab. Special emphasis will be made in IV test, visual inspection and electrical test, the

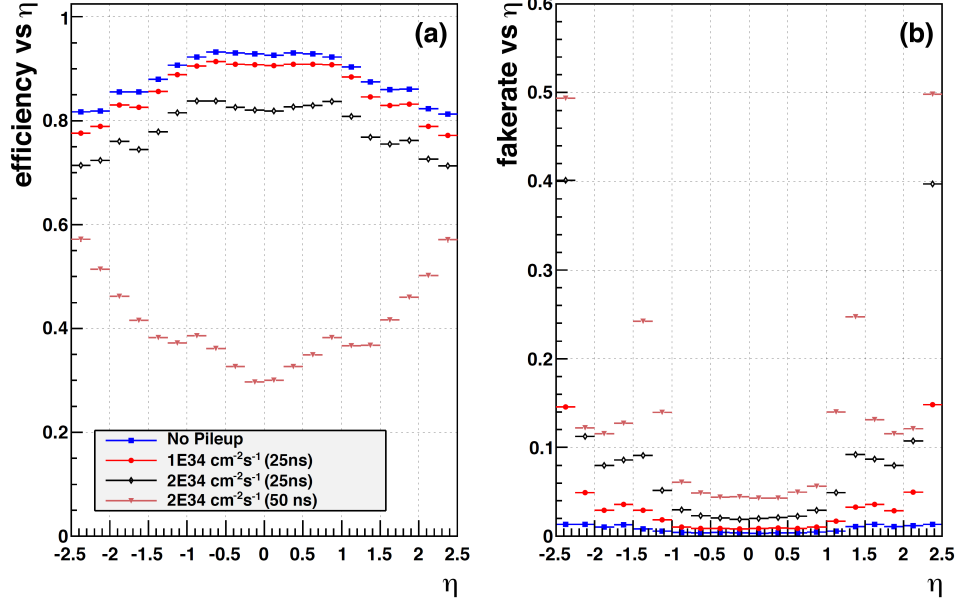


Figure 7.1: Expected performance of the original pixel detector under different luminosity conditions: a) track-finding efficiency; b) fake rate. Conventions are the same for both plots, considering zero pileup (blue squares), average pileup of 25 (red dots), average pileup of 50 (black diamonds), and average pileup of 100 (magenta triangles). [5]

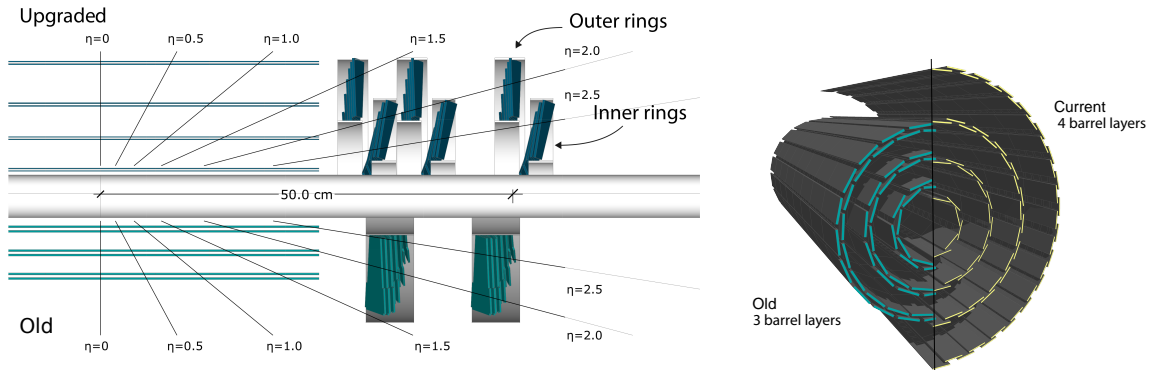


Figure 7.2: Layout and comparison of the layers and disks in the upgraded (Phase I) and old (Phase 0) pixel detectors [5].

stages where the author of this work made a lot of contributions [improve](#).

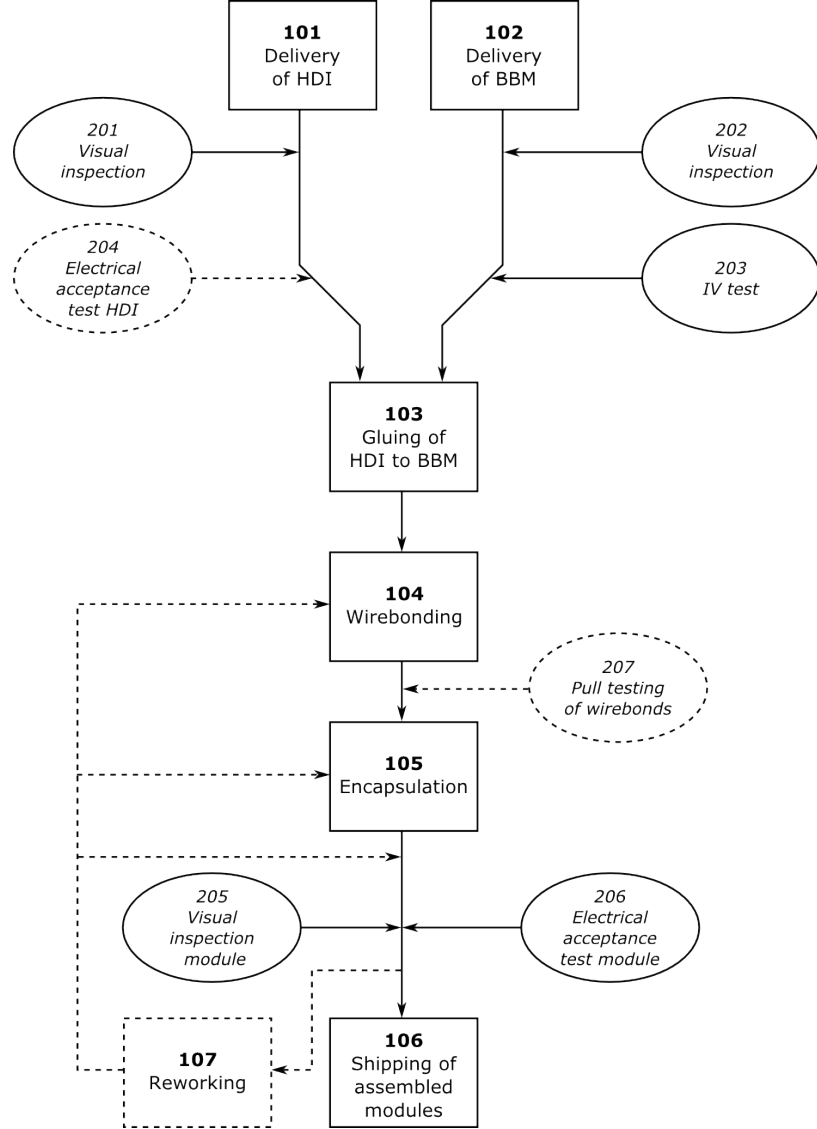


Figure 7.3: UNL module assembly workflow. Dashed lines represent occasional quality testing and reworking procedures [6].

7.2.1 Visual Inspections

The UNL-HEP group assembly workflow started upon receiving two components: a Bare Bonded Module (BBM) and a High Density Interconnect (HDI), see figure 7.4. The first stage of the module production was a visual inspection on these components to ensure they were in good conditions and able to continue into the production

pipeline.

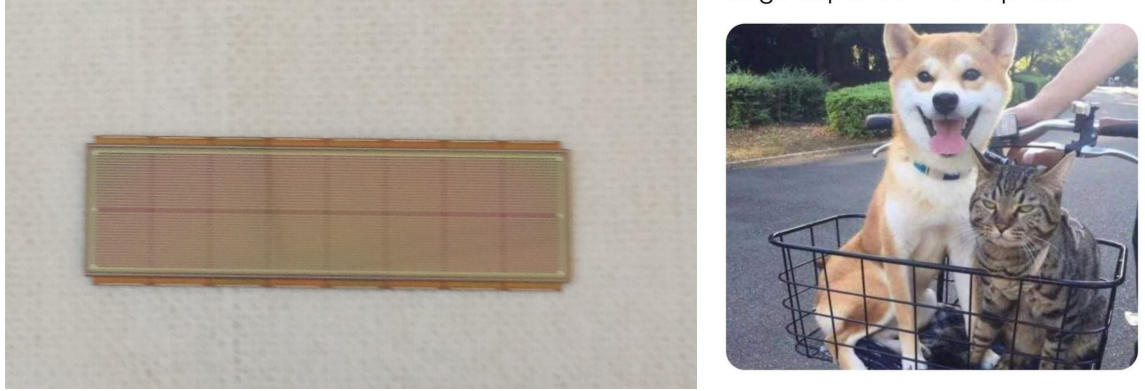


Figure 7.4: Photograph of a BBM (left) and HDI [right one](#)(right) as received by the UNL-HEP group.

To get a good view of such a small components a powerful microscope with magnification of [confirm](#), an attached camera, and LED ring illumination was used. A photograph of the set up, also referred to as probe station, is shown in figure 7.5. The entire set up was connected to a vacuum line to secure these component in place and avoid any damage during the visual inspection. BBMs were received in a gel pack while HDIs were usually received in their modules carriers. BBMs and HDIs were then moved into the probe station using a vacuum pen and taking the appropriate safety precaution: ESD wristband, gloves, face mask, etc.

During visual inspection BBMs were scanned for unusual features or sign of damage, special attention was given to the high voltage connection and bond pads. Figure 7.6 shows different parts of four different modules where defects on three of them could be observed. Some of these defects, bottom right figure, caused the module to be rejected immediately while others, bottom figures, will still undergo an IV test. While for the HDI the bond pads of the 16 ROCs, the wirebonds of the tbm, and the address pads were carefully checked. Figure 7.7 shows the TBM wirebonds as well as

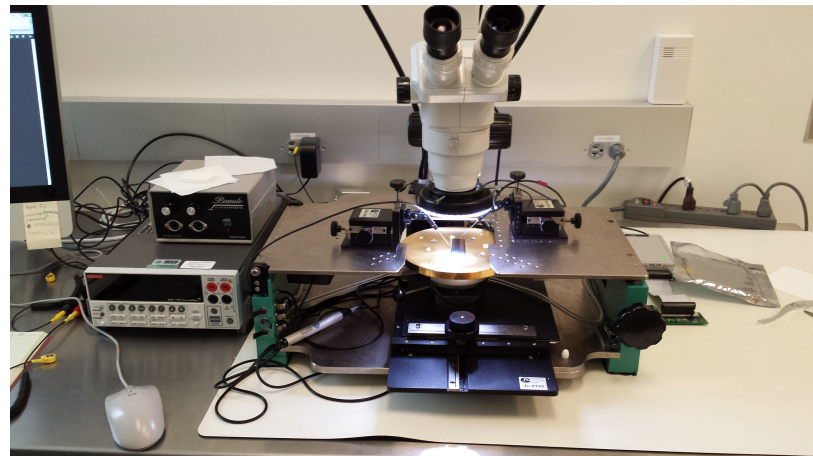


Figure 7.5: fix Photograph showing a BBM under the microscope during a visual inspection. This station also served as IV test stand.

the bondpads of a ROC in a HDI.

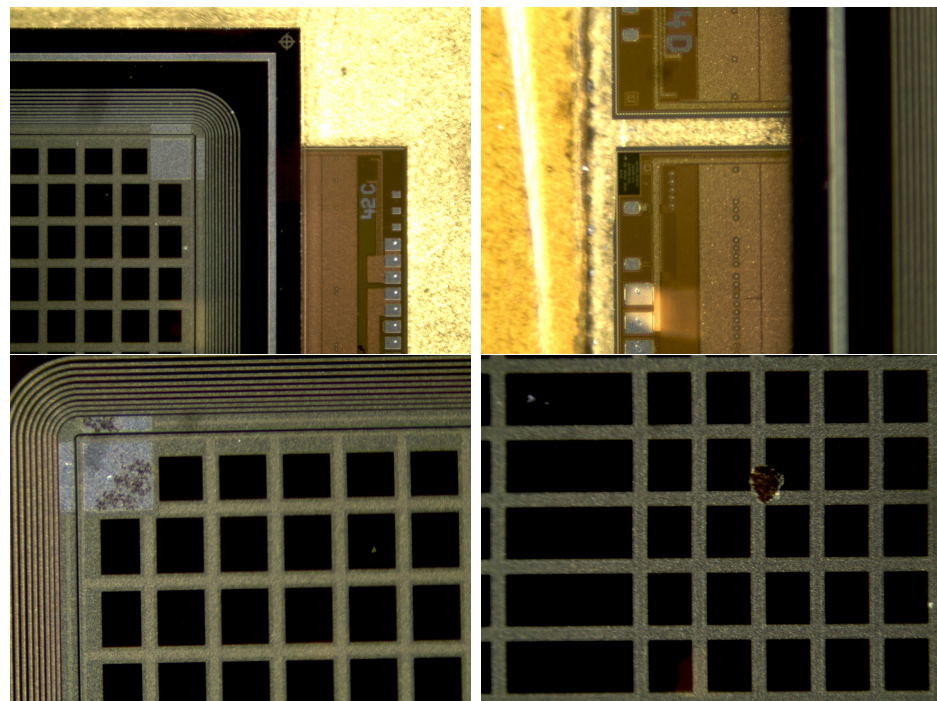


Figure 7.6: Photograph of the visual inspection of a BBM showing few of the things observed during a visual inspection: A good module (top left), chipped ROC (top right), scratches on the high voltage connection pad (bottom left), and scratch on the midle of a ROC (bottom left)

Figures 7.6 and Fig. 7.7 also show a trend that was observed throughout the

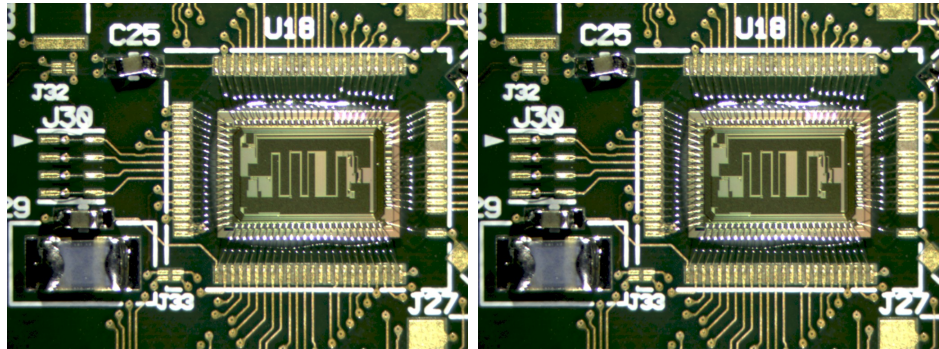


Figure 7.7: Photograph of the visual inspection of a HDI shwing the wirebonds of the TBM (left) and the bondpads of a ROC (right). [right fig](#)

entire production phase. In general more unusual features and damage were observed in BBMs than on HDI. This was because BBM were derivered directly from the production company to our lab while HDIs were first delivered to the Fermi National Laboratory (FermiLab) where they were preliminary tested and inspected before they arrive at our testing facilities.

7.2.2 IV Test

After both BBM and HDI have succesfully passed the visual inspection the BBM continues to the probe station for a current vs voltage (IV) test. The test uses the fact that the sensor behaves like a diode. During operation a potential difference is applied to the sensor to draw the electrons created by a charge particle passing through the sensor towards the bump bond to be collected. If this potential difference is too small not all electron will collected in time and if it is large the sensor could break. This potential difference is known as a depletion voltage. The IV test is meant to find the operating range, a voltage where all the electron could be collected and the sensor will not break, for a given module (sensor). Figure 7.8 (left) shows the position of the probes to perform an IV on a BBM and figure 7.8 (right) shows IV results for a BBM in good operating condition.

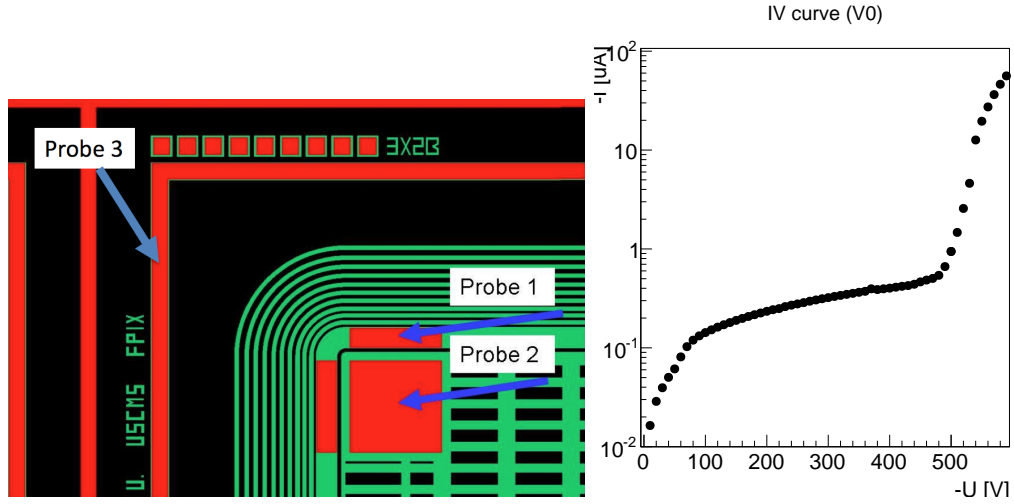


Figure 7.8: Left: Probe position for an IV test on a BBM. Probe 2 is high voltage, probe 3 is ground, and probe 1 was not used [6]. Right: IV test results for a good BBM. The depletion voltage for this module is around [confirm with right picture](#).

7.2.3 Gluing

The gluing routine was carefully designed to perfectly match the HDI and BBM bond-pads, in preparation for the wirebonding. This stage of the production was done using a custom made gantry, *AGS15000 Series Gantry*, fabricated by Aerotech [9]. It offered translational motion in 3D as well as rotation in x-y (gantry table) plane. A camera was attached to the gantry head allowing the user to monitor the entire process. This camera was of particular importance during the development and improvement of the gluing and encapsulation routine. A video showing the gluing routine in action can be watched at [8] and a full description of the gluing routine and procedure can be found in [7]. Figure 7.9 shows the gantry with the different tools used to glue a HDI on a BBM. The final product after the process is completed can be seen in Fig. 7.10.

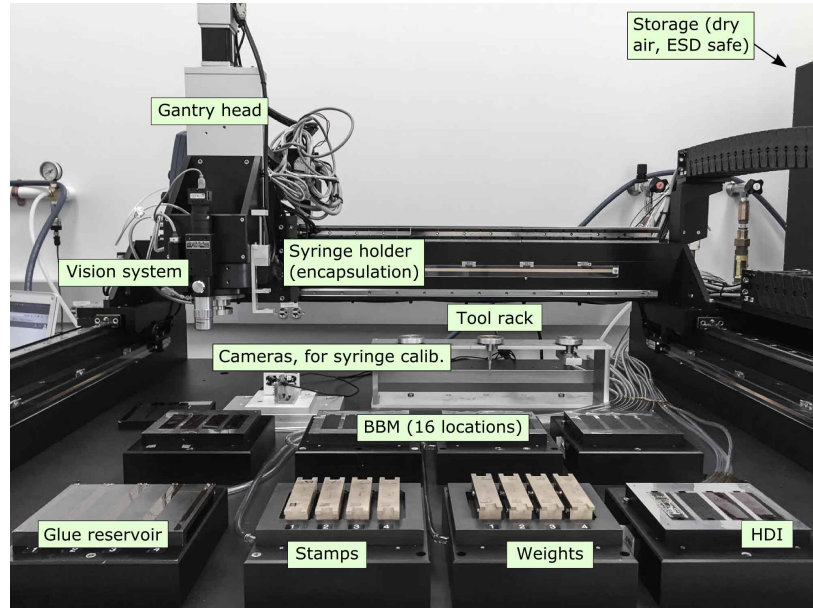


Figure 7.9: Photograph of a gantry used for gluing and encapsulation showing different parts of the set up and tools.

7.2.4 Wirebonding

After an HDI is glued to a BBM the next step in the assembly process is to make electrical connection between them.

7.2.5 Encapsulation

The final step in manufacturing a module is to protect (cover) the wirebonds with an encapsulant, wirebond encapsulation. This procedure is necessary to ensure that the wirebonds are secure at both HDI and BBM ends. The set up and the equipment used is the same as for gluing showed in figure 7.9. Additional materials needed for this step are shown in figure 7.13.

A material suitable for this task must be radiation hard and lightweight among other properties. After testing different material and alloys we settle on *Silgard 186*, a mixture of two-component encapsulant. Erastomer (10 cc) and elastomer (1 cc)



Figure 7.10: HDI glued on top of a BBM. For a batch of four modules (top) and zoom in view to note the almost perfect alignment between the HDI and BBM bondpads.

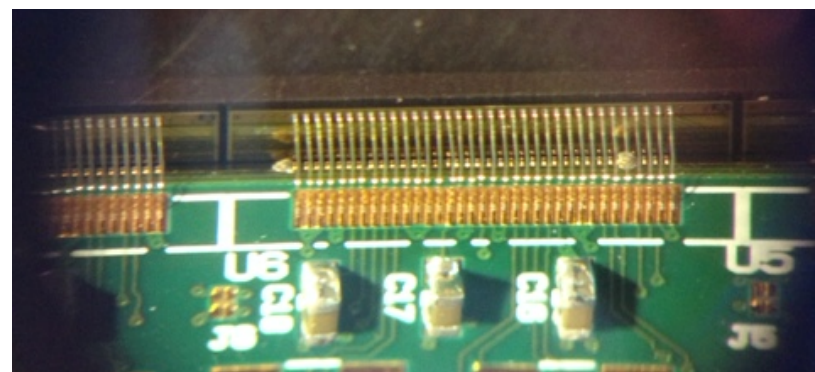


Figure 7.11: Wirebonding set up [find fig.](#)

base and curing agent respectively. The components then, were mix together using a centrifuge and place in a syringe for dispensing. There are three components that need encapsulation, HDI and BBM bond pads, TBM wirebonds, and high votage pads.

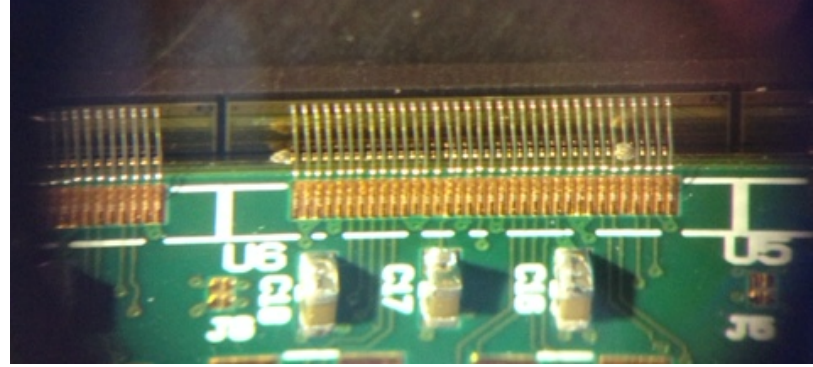


Figure 7.12: Close up view of the wirebonds for a single ROC on a wirebonded module.

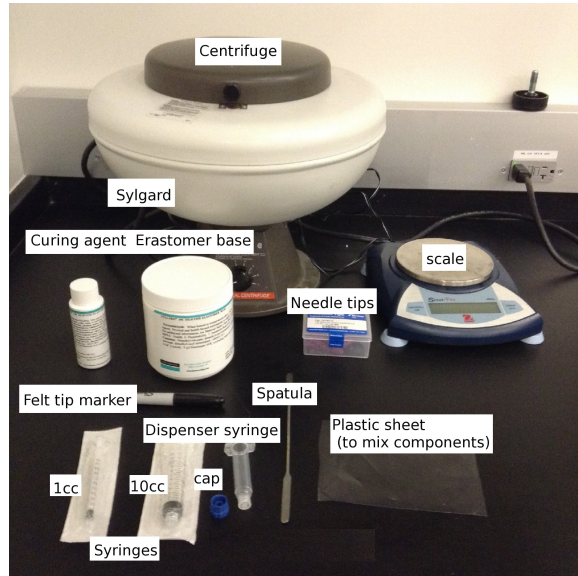


Figure 7.13: Wirebonds encapsulation materials [6].

Figure 7.14 shows a module after its different components have been encapsulated. Note how all bond foots and pads are fully covered as needed [7].

7.2.6 Electrical Test of a Fully assembly Module

A manufactured module can be seen in Figure 7.15, it is then visually inspected and mark as ready for electrical test **at the end of previous session?**. The electrical test, hereon fulltest, of fully assembly modules is done using the *pXar* software framework,

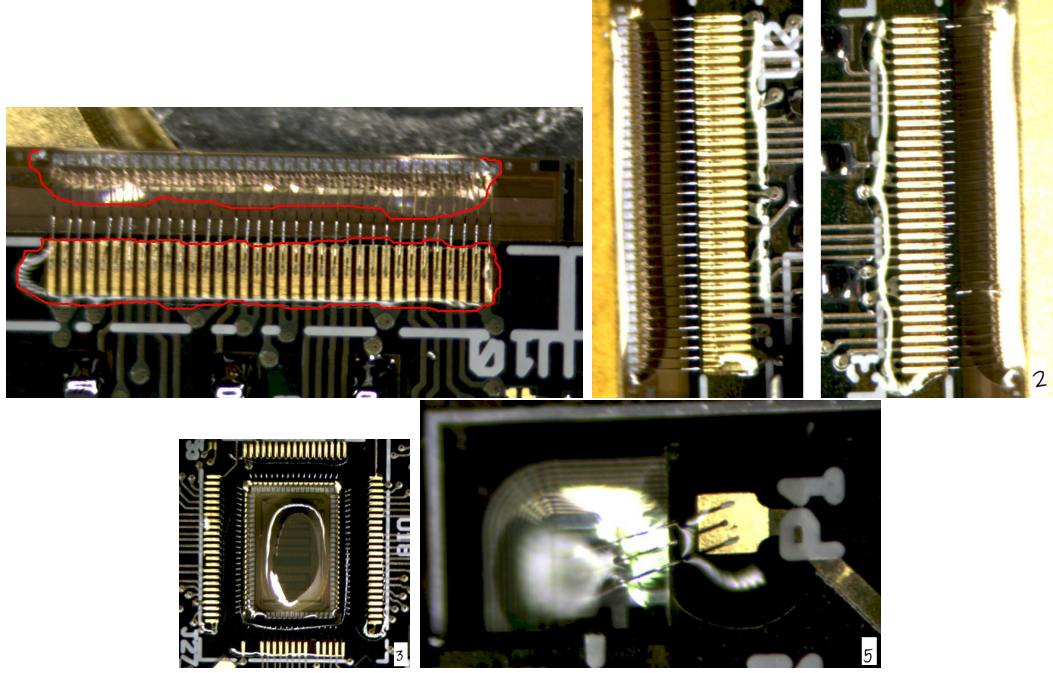


Figure 7.14: Wirebonds encapsulation of the components of a module. Top left, roc used as reference, the boundaries of the encapsulant are enhanced with red lines for better visibility. Top right, two ROCs on two different modules side by side, b) encapsulation of TBM, c) encapsulation of the high voltage pad.

written by the CMS FPix collaboration. More information on *pXar* can be found in [11]. The objective of the *Fulltest* is to ensure that all 16 ROCs were functional and have good performance. For this purpose a suit of several tests were designed and developed, the software is flexible in the sense that we could execute a single test just by calling its name or we could execute them all with a single command *Fulltest*. The *Fulltest* at UNL was done using the set up showing in figure 7.16 at a temperature of $17^\circ C$ and using a depletion voltage of $-150 V$.

The following section [subsections?](#) give a short description of the most *important* tests a module has to surpass as well as the output of these test. A full list of the tests, a comprehensive description of them, and a [description](#) of their purpose can be found in [12] and references therein. After the *Fulltest* of modules was completed some were shipped to Kansas university for X-ray testing and the rest were shipped

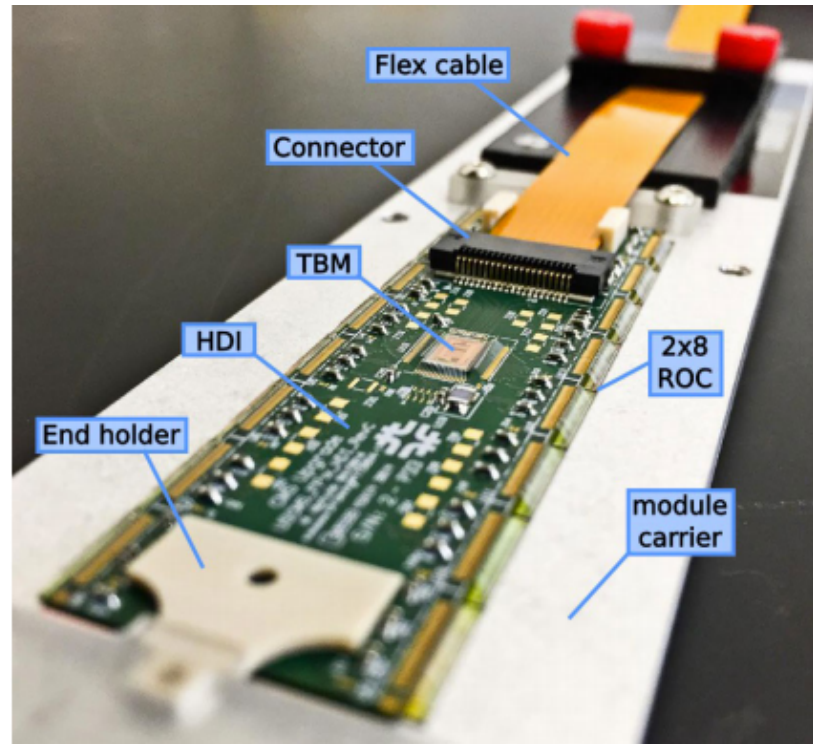


Figure 7.15: Fully assembly Module

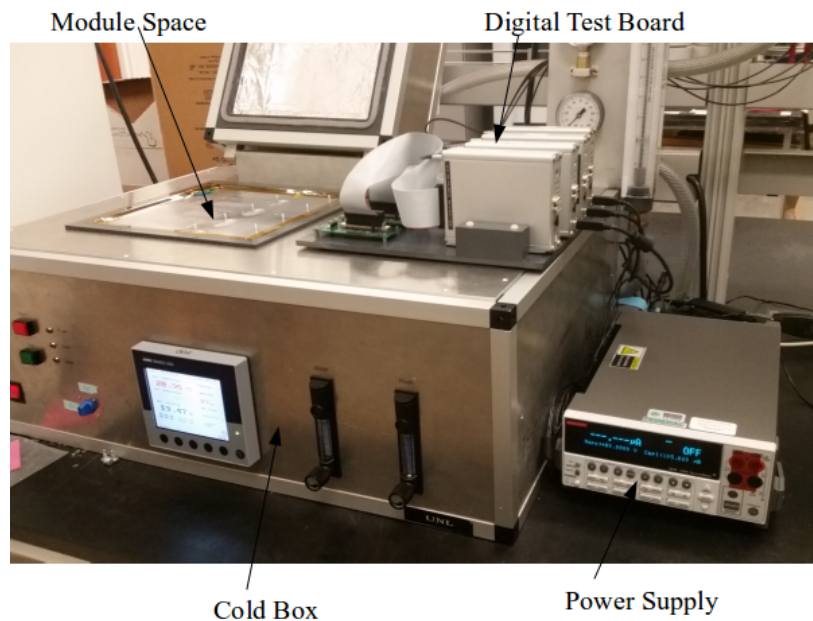


Figure 7.16: Fully assembly module testing set up

to FermiLab for testing at $-10^\circ C$

7.2.6.1 IV Test

A fully assembled module also undergoes an IV test as described in 7.2.2. The primary purpose of this test is to ensure that no damage was caused to the circuitry during the assembly process and the module could be operated at high voltages. The IV result for a sample module is shown in figure 7.17. The operational range for this particular module is between -100 V and -400 V.

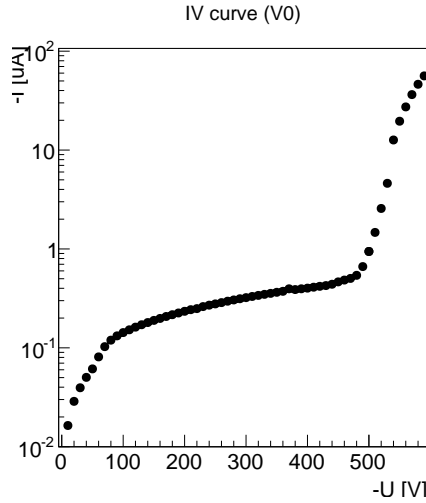


Figure 7.17: IV test for a fully assembly module.

7.2.6.2 Pretest

It is composed of several subtests and its purpose is to check the basic functionalities of the ROCs and to calibrate some of the DAC [list of DAC here or in ch 2?](#) settings. A couple of these subtests are *ProgramRoc* and *SetVthrCompCalDel*. The *ProgramRoc* measures the difference in current (I_{ana}) drawn by the amplifiers when a voltage (V_{ana}) is applied and removed. If the difference between these two measurements is non-zero it implies that we are able to change DAC values by sending a command,

the ROC is programmable. This test is done for all 16 modules in a ROC. The *SetVthrCompCalDel* subtest is done to optimize the value of the VthrComp and CalDel DACs. It chooses a pixel from within a ROC and sends 5 calibration pulses to the PUC of this pixel. This process is repeated for the 256 x 256 parameter space of these DACs and the response of the pixel is read to make an efficiency plot. Then VthrComp is set to the lower plateau plus 50 units and CalDel is set to half of the left and right edges. This is known as the *VthrComp* and *CalDel* working point of the pixel. Figure 7.18 shows the output of these subtests for a sample module

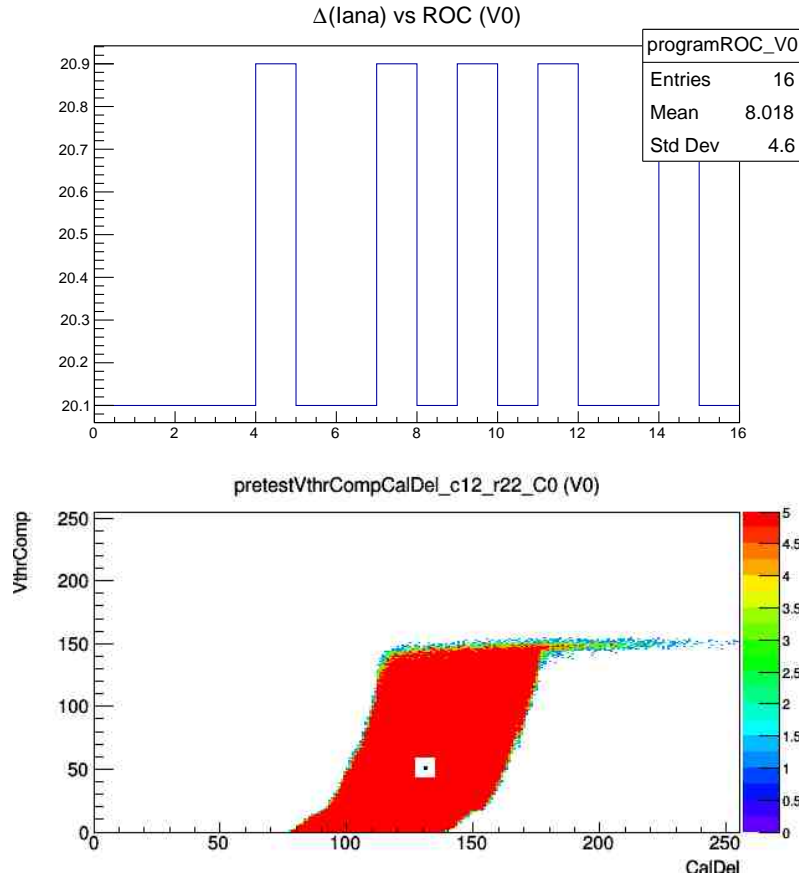


Figure 7.18: Output of the ProgramRoc (left) and finding working pixel (right) subtests.

7.2.6.3 Pixel Alive

In the pixel alive test three subtests are performed: *Alive test* checks for the response of a pixel by sending 10 calibration pulses (hits) to it and recording how many the pixel reports back. Pixel with 10 hits are marked as good, those with less than 10 hits are flagged as faulty, and those with zero hits are called dead. In the *Mask test* all pixels are disable and the same efficiency measurement is done. Pixels with zero efficiency are marked as good while those with efficiency grater than zero are bad. The *AddressDecoding* test checks the specific address of the pixel within the ROC. If the response of the pixel does not match the address to which it was sent the pixel is marked as bad. repeats the same procedure but checks that the order of the resulting data. If the address of a given pixel is out of order, the recorded hit is given a negative pulse height value. Pixels with negative hits are flagged as faulty. Figure 7.19 shows the result of the pixel alive test for a fully working module and Figure 7.20 shows a module with faulty ROC and a ROC with faulty pixels.

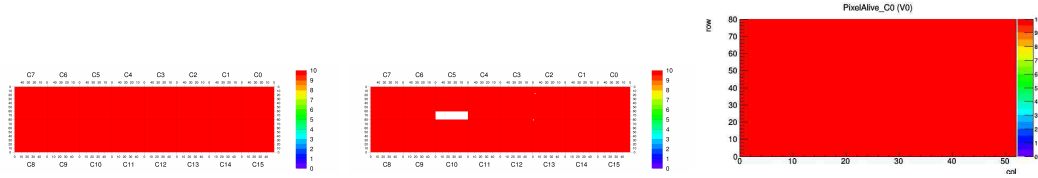


Figure 7.19: Pixel alive test for a fully assembled module. a) Alive test, b) Mask test, and c) AddressDecoding test.

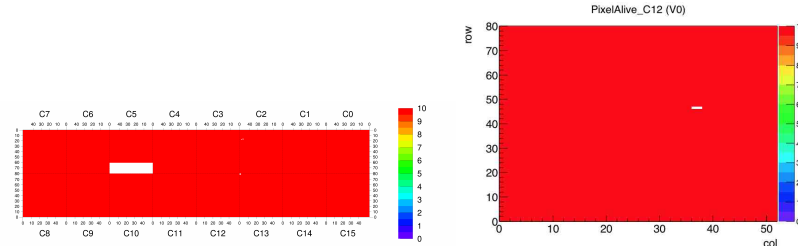


Figure 7.20: Pixel alive for a fully assembled module. a) a module with a faulty ROC and b) a ROC with faulty/dead pixels

7.2.6.4 Trimming Test

The aim of the the trimming test is to (calibrate) set the threshold of all pixel on a ROC as uniform as possible. It attempts to do this by varying the VthrComp, Vtrim, and Trim bits DACs. The Trimming test sets VthrComp and Vtrim for the entire ROC and then uses trim bits to further refined the threshold of individual pixels. After the trimming test is finished all pixels within the ROC **will have a threshold value as low as possible but still higher than the electrical noise**. Furthermore, a TrimBits subtest verifies that all trim bits are working by sequentially enabling each bit and observing its effect on the pixel threshold distribution. The trimming test works as follows: first, with Vcal set to a target value, it finds the VthrComp turn-on value by producing S-Curves for all pixels with respect to VthrComp. Then, VthrComp is set to the value of the pixel with the lowest turn-on value. A ROC map distribution of turn on values for a ROC can be seen in figure 7.21. Then, with the VthrComp set to its lowest value, the test tries to minimize the Vtrim value by repeating the previous process and finding the pixel with the highest Vcal turn-on value, see Fig 7.21. This is the pixel that requires the most trimming to have its Vcal threshold reduced to the target value. Following, with all trim bits enabled, the test performs an efficiency scan over Vtrim and Vcal DACs 7.21 to find the value of Vtrim that corresponds to a turn-on at the target Vcal.

Next, starting from a high Vtrim, its value is iteratively lowered until the Vcal turn-on surpasses the target Vcal, which corresponds to the minimum value that can trim this pixel. This is the final value of the Vtrim DAC for the the ROC. Finally, with the values of the VthrCaomp and Vtrim set, the test refine the threshold on each pixel by modifying the 4 Trim bits. Starting with the Trim bits set to 7 [0111], scurves are used to find the Vcal turn-on value. If the pixel **reports a hit** fires below (above)

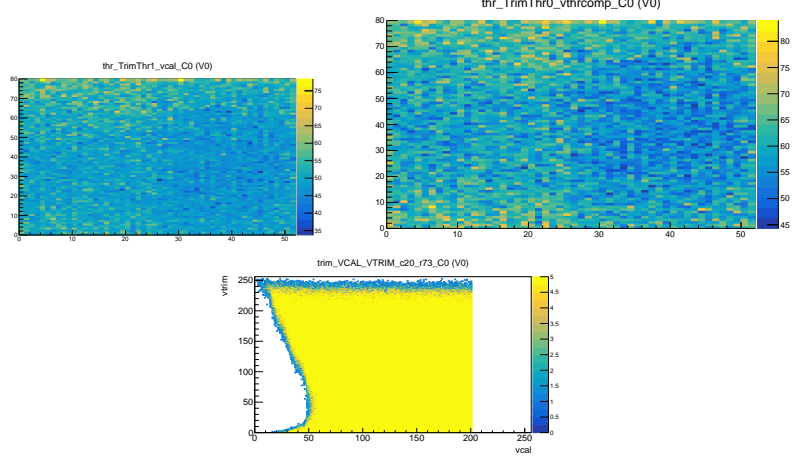


Figure 7.21: Trim test optimization for. left: Vcal turn on, center: Vthr turn on, right: efficiency in the Vtrim-Vcal plane.

the target Vcal value, the Trim bits value is increased (decreased) by 4, so that the amount of trimming is decreased (increased). This process is repeated three more time increasing or decreasing the Trim bits values by 2, 1, and 1 unit respectively, covering the full range, 0-15, of the Trim bits. Figure 7.22 shows a ROC map of Vcal for Trim bits = 7 and after 4 corrections are made and the final Vcal map and distribution could be seen in figure 7.23.

7.2.6.5 PH Optimization

7.2.6.6 Gain Pedestal

7.2.6.7 Scurve Test

The SCurve test measures the efficiency of a pixel as a function of Vcal. It is based on the assumption that a pixel will not respond to lower values of Vcal but it will always respond for higher values. In the absence of noise this curve will be just a step function which changes from zero efficiency below the threshold to a region of 100% efficiency above. The effect of the noise is to smear out the step function giving it a *S*

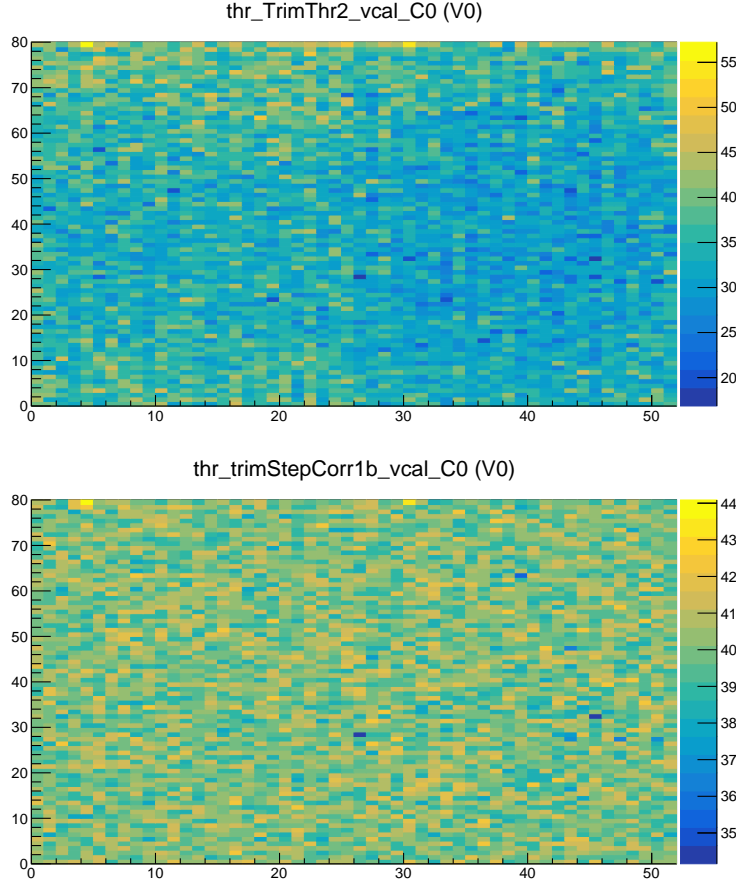


Figure 7.22: Trim bits map distributions for the Vcal turn-on values for the initial and final Trim bits values.

shape. As the noise is assumed to follow a Gaussian distribution, the SCurve if fitted with an error function and its width is a measure of the noise level in the pixel. Since the Vcal is known at this point in the testing procedure the SCurve is done around this Vcal value. In order to extract an accurate estimate of the width the number of triggers used for the test is 200. The output of this test can be seen in figure ??

7.2.6.8 Bond Bonding Test

could be better, include the ROC-Sensor air gap? The primary purpose of the *Bump-Bonding test* is to identify problems with the bumps connecting the sensor to the

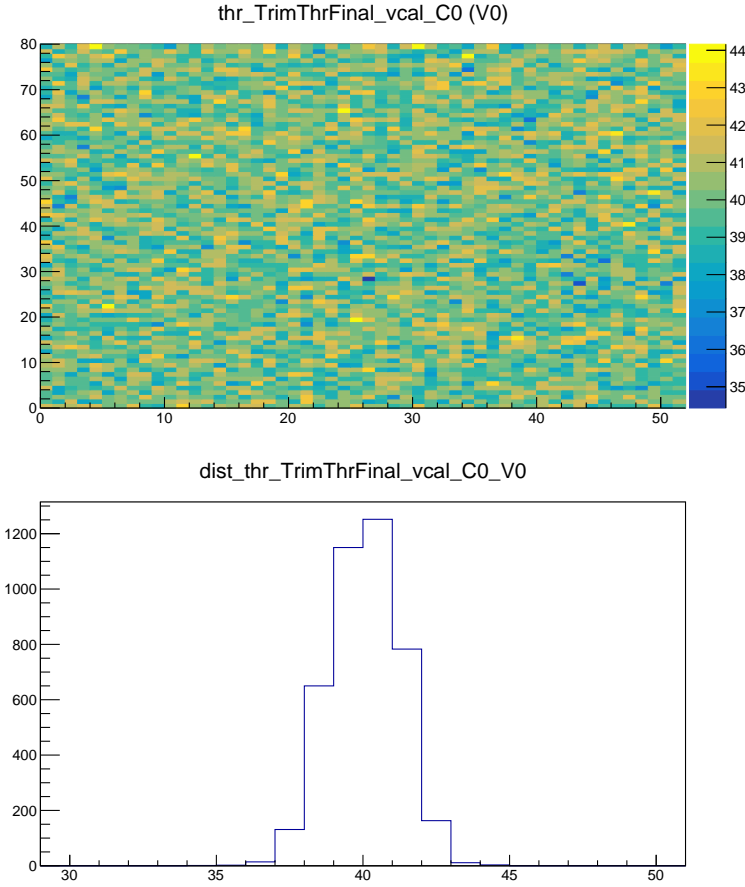


Figure 7.23: Final map and distribution of Vcal threshold after the Trim test have finished.

ROC. The test works by a calibration signal to the sensor via the alternatively path labeled 'sensor calib' 7.26. The signal then reaches the sensor and makes its way to the ROC via the bump bond where it can be normally read. The strength of the signal is measure and compare to the one sent. In the *pXar* software usually 5 signal of 250 Vcal units are sent to each pixel during a *BumpBonding* test. The **output** of the test is shown if figure 7.25

7.2.6.9 Summary

The UNL-HEP module production was a susceesful project that culminated with the production and testing of over 500 modules. team

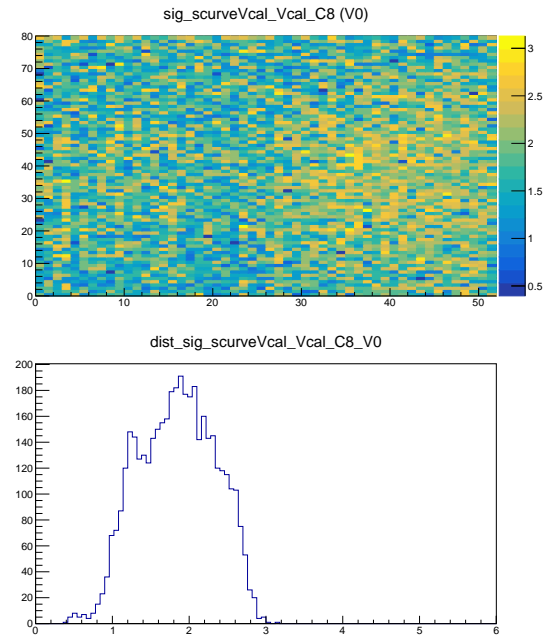


Figure 7.24: Left: ROC map of the Vcal s-curve turn-on widths. Right: 1D distribution of the vcal scurve width.

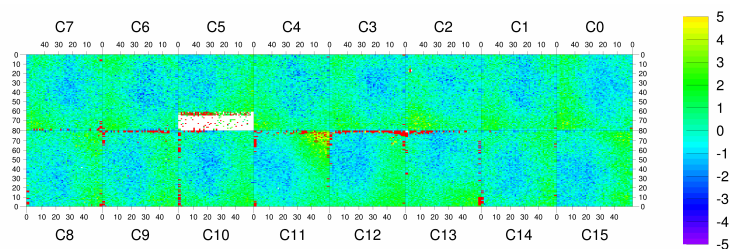


Figure 7.25: Bond bonding test.

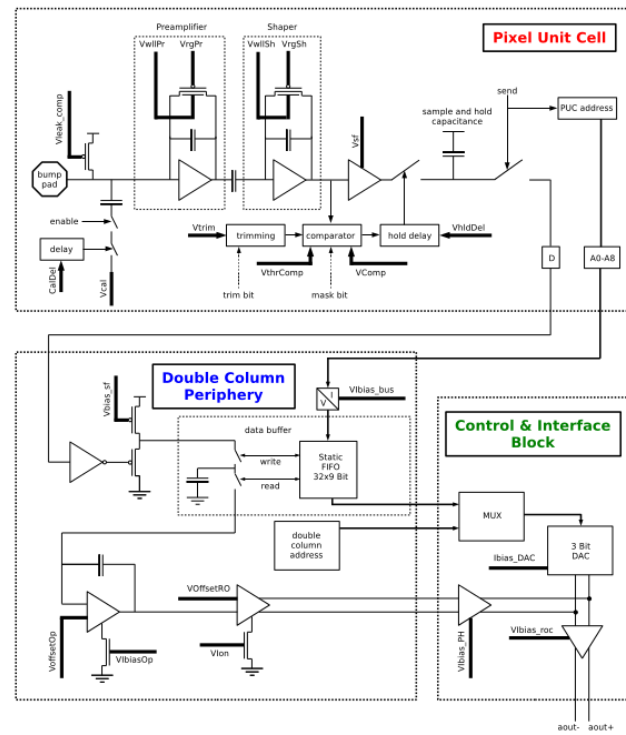


Figure 4. Schematic view of the readout chain

Figure 7.26: Pixel unit cell find calibration figure.

CHAPTER 8

Beam Test of the RD53 chip for CMS Pixel Detector Upgrade Phase 2

8.1 Introduction

8.2 The RD53 Chip

8.3 Purpose of Test Beam

8.4 Test Beam Set Up

8.5 Results

CHAPTER 9

Conclusions

9.1 Analysis

9.2 Phase 1

9.3 Beam Test

References

- [1] The Atlas collaboration, Technical Design Report LHCC 99-14, ATLAS TDR 14. CERN, Geneva Switzerland, 1999
- [2] CMS Collaboration. The CMS Experiment at the CERN LHC. Volume 3, 2008.
- [3] LHCb Collaboration, S. Amato et al., LHCb technical proposal,CERN-LHCC-98-04
- [4] ALICE: Technical proposal for a large ion collider experiment at the CERN LHC, CERN-LHCC-95-71.
- [5] A. Dominguez et. al. “CMS Technical Design Report for the Pixel Detector Upgrade”, CERN-LHCC-2012-016. CMS-TDR-11.
- [6] UNL Phase I FPIX Assembly Standard Operating Procedures. From <https://github.com/psi46/unl-sop>, 2016.
- [7] J. Monroy. Search for production of a Higgs boson and a single top quark in multilepton final states in pp collisions at $\sqrt{s} = 13$ TeV July 2018.
- [8] F. Meier “ Forward Pixel Module Glueing at UNL” YouTube, Sep. 15, 2014, from <https://www.youtube.com/watch?v=ofdntTIwKY4>.

- [9] Aerotech (n.d). “AGS15000 Series”, from <https://www.aerotech.com/product-catalog/gantry-system/ags15000.aspx?p=%2fproduct-catalog%2fgantry-system.aspx%3f>
- [10] J. Monroy (n.d). Home [YouTube Channel]. from <https://www.youtube.com/channel/UCi7S7vhYpieL0y2KJ0SS0eg>.
- [11] pXar software framework 2015, from <https://twiki.cern.ch/twiki/bin/viewauth/CMS/Pxar>.
- [12] J. Antonelli. “FPix Module Testing Reference Guide”, Sep. 2015, from <https://cms-docdb.cern.ch/cgi-bin/DocDB/RetrieveFile?docid=12690&filename=fpix-module-testing-reference-guide.pdf&version=5>